Flow distribution analysis as a probe of nuclear deformation

Hadi Mehrabpour [1,*] and S. M. A. Tabatabaee [2,†]

[1] *PRISMA⁺ Cluster of Excellence & Mainz Institute for Theoretical Physics, Johannes Gutenberg-Universität Mainz, 55099 Mainz, Germany*

[2] *School of Particles and Accelerators, Institute for Research in Fundamental Sciences (IPM), P.O. Box 19395-5531, Tehran, Iran*

(Received 19 February 2023; revised 3 July 2023; accepted 23 August 2023; published 1 September 2023)

We study the flow harmonic distribution in collisions of deformed nuclei. To do this, we use the standard Gram-Charlier method to find the higher-order correction to the well-known Bessel-Gaussian distribution. We find that, apart from the necessity of including a shift parameter $\bar{v}_n$, the modified flow distribution accurately describes the distribution of flow harmonics in a system formed after collisions of deformed nuclei with quadrupole and octupole deformity. Using the shifted radial distribution arising from this method, we scrutinize the effect of deformation on flow distribution. We also propose a way to measure $\bar{v}_2$ in deformed-nucleus collisions.

DOI: 10.1103/PhysRevC.108.034902

I. INTRODUCTION

Quantum chromodynamics (QCD), the theory of the strong interaction, undergoes a certain phase transition at high temperature to a plasma of quarks and gluons. Heavy-ion collisions (HICs) at the BNL Relativistic Heavy Ion Collider (RHIC) and Large Hadron Collider (LHC) provide this opportunity to study the phase structure of QCD and the properties of quark-gluon plasma (QGP) [1–8]. One feature of this plasma is collective behavior which can be successfully described by the hydrodynamic models [9]. Among the various probes to study the dynamics of relativistic HICs, the most used one is the anisotropic flow that is quantified with harmonics v_n, measuring the azimuthal asymmetry of the emitted hadrons on an event-by-event basis. The flow distribution and the cumulants are used to gain more information on the even-by-event fluctuations [10]. This insight shed light on the collision geometry, quantum fluctuations at initial state, as well as the effects of different evolution stages in heavy-ion processes [11,12]. From an experimental point of view, the distribution of v_2 and v_3 are accessible through the unfolding method [13]. This leads to an observation of a Bessel-Gaussian distribution for collision of spherical nuclei, i.e., Pb-Pb, in the central collision [14]. On the other hand, cumulants can be obtained as a measure of multiparticle correlation functions [15]. Measuring the correlation of particles gives this chance to map the shape of nuclei [16].

Conventionally, in low-energy nuclear physics, a Woods-Saxon profile describes the density of nucleons inside a nucleus,

$$\rho(r,\theta,\phi) \propto \frac{1}{1+e^{\frac{r-R(\theta,\phi)}{a_0}}}, \tag{1}$$

where a_0 and $R(\theta,\phi)$ are the surface diffuseness and the nuclear surface parameter, respectively. In general, to take into account the deformation of the nucleus, $R(\theta,\phi)$ is expanded in terms of spherical harmonics $Y_\ell^m(\theta,\phi)$. In particular, the quadrupole deformation in the so-called real spherical harmonics is defined by $R(\theta,\phi) = R_0\{1+\beta_2[\cos\gamma Y_2^0(\theta,\phi) + \sin\gamma Y_2^2(\theta,\phi)]\}$ [17]. Here, R_0 is the half-density radius, γ determines the relative length of the three axes of the ellipsoid, and β_2 is the magnitude of quadrupole deformation. From an experimental point of view, there are some pieces of evidence that support a considerable difference in observed v_2 of final particles in a system formed after the collisions of deformed and spherical nuclei [18], with the largest difference being in the most central collisions. Besides the quadrupole deformation, octupole deformation may also significantly affect observables. This form of deformation arises due to the breaking of parity symmetry in the intrinsic nuclear shape. This kind of deformity is modeled by including $\beta_3 Y_3^0(\theta,\phi)$ in the nuclear surface parameter.

The structure of this paper is as follows: In Sec. II, we present a brief review of the standard Gram-Charlier series method. Using this approach, we find the cumulants of flow harmonics in Sec. III. We argue that, to include the effect of deformation on the cumulants, we have to consider a shift parameter in the definition. Then we obtain the flow distribution for the magnitude of flow harmonics, which is dubbed as the radial flow distribution. We observe that the conventional Bessel-Gaussian is not appropriate for the central collisions. Once we consider higher-order corrections, i.e., fourth- and sixth-order radial cumulants, the data are explained accurately. We show that the first correction due to the fourth-order term, which turns out to be kurtosis of the v_n event-by-event fluctuation [19], is sufficient. In Sec. IV, we present an approach to observe the shift parameter in experiments. We summarize in Sec. V and present our concluding remarks.

II. METHOD OF ANALYSIS

In this section, we use the so-called standard Gram-Charlier (sGC) series to find the distribution of any random variable. In case where the related information of the desired

*mehrabph@uni-mainz.de

†tabatabaee@ipm.ir

 ©2023 American Physical Society

variable, such as its moments, is incompatible with Gaussian distributions, this series can be used to modify Gaussian distributions. This method relates the probability distribution $P(\mathbf{Z})$ to the Gaussian distribution by applying an appropriate differential operator [20–22]. It is worth mentioning that this approach, at first, was used in Ref. [19] to study the flow distribution.

Let us start with the characteristic function $\Phi_{\mathbf{Z}}(\mathbf{t})$ of a k-dimensional random vector $\mathbf{Z}$, which is defined as

$$\Phi_{\mathbf{Z}}(\mathbf{t}) = \int d\mathbf{Z} e^{i\mathbf{t}^T\mathbf{Z}} P(\mathbf{Z}). \tag{2}$$

Here, $\mathbf{t}$ belongs to $\mathcal{C}^k$ ($\mathcal{R}^k$) when $\mathbf{Z}$ is complex (real). As it turns out, if the random vector $\mathbf{Z}$ has a moment-generating function $\mathcal{M}$, the domain of the characteristic function can be extended to the complex plane, and we have $\Phi(-i\mathbf{t}) = \mathcal{M}(\mathbf{t})$. Moreover, an alternative definition of the second characteristic function $\mathcal{M}(\mathbf{t})$ is given by $\mathcal{K}(\mathbf{t}) = \ln \mathcal{M}(\mathbf{t})$. Thus, this leads to the cumulants of the random vector as $\mathcal{K}^{(n)}(\mathbf{t})|_{t=0} = [\ln \mathcal{M}(\mathbf{t})]^{(n)}|_{\mathbf{t}=0}$.[1] Furthermore, the probability function defined in Eq. (2) is determined by an inverse Fourier transformation [21] as follows:

$$P(\mathbf{Z}) = \frac{1}{2\pi} \int d\mathbf{t} e^{-i\mathbf{t}^T\mathbf{Z}} \Phi_{\mathbf{Z}}(\mathbf{t}). \tag{3}$$

Expanding the characteristic function up to second order and writing $(i\mathbf{Z})^n$ in terms of an appropriate differential operator, we arrive at an expression for $P(\mathbf{Z})$. Following the steps described above to find the distribution function for a real random variable x, we find the corrections to the conventional Gaussian distribution. The corresponding terms are given in terms of the probabilist Hermite polynomials He_n as

$$\sum_{n=3}^{\infty} \frac{\kappa_n}{n!\sigma^n} He_n\left(\frac{x-\mu}{\sigma}\right).$$

The sGC method aims to find the non-Gaussianity correction to obtain a complete description of our variable. This leads us to focus on the characteristic function instead. Since this quantity gives us the desired information about the moments and cumulants, it provides insight into the probability distribution. It is known that both collision geometry and event-by-event fluctuations are encoded in flow harmonic distributions $P(v_n)$ as well as cumulants [23]. In the following sections, we study the connection between them to gain a deeper insight into the effects of nucleus deformation using sGC series in the two cases of spherical- and deformed-ion collisions.

[1]Assuming a real random variable x the corresponding equation leads to:

$$1 + \sum_{n=1}^{\infty} \frac{\mu_n t^n}{n!} = \exp\left(\sum_{n=1}^{\infty} \frac{\kappa_n t^n}{n!}\right),$$

where for a particular choice $\mu = \langle x \rangle$, it implies

$$\mu_1 = \mu = \kappa_1,$$

$$\mu_2 = \mu^2 + \sigma^2 = {\kappa_1}^2 + \kappa_2,$$

$$\mu_3 = \mu^3 + 3\mu\sigma^2 + \kappa_3 = {k_1}^3 + 3\kappa_1\kappa_2 + \kappa_3.$$

III. SPHERICAL- AND DEFORMED-NUCLEUS COLLISIONS

In this section, we examine the effect of deformation on the flow anisotropy. To start, we present the $2k$-particle correlation functions $c_n\{2k\}$ [15] as well as the shifted cumulants [24] for the collision of spherical and deformed ions. The present work aims to study the effects of deformation on cumulants, resulting from the initial stage of collision of nuclei. To do this, we use the approximate relation between v_n and the initial anisotropy ε_n for second and third harmonics: $v_n = \alpha_n \varepsilon_n$ [25,26]. Therefore, we do not need to compute v_2 and v_3 by means of full hydrodynamic simulations. α_n is a response coefficient that depends on the properties of the medium, such as its viscosity. In this paper we assume that, at a given centrality, this coefficient is same for all events.[2] Its value has been determined at both RHIC and LHC energies (see Ref. [27]). Thus, we have generated data for PbPb and UU as well as ZrZr collisions at the center-of-mass energy $\sqrt{s_{NN}} = 5.02$ TeV and 200 GeV, respectively, motivated by LHC [28] and RHIC [18] experiments.[3] To do this, we implement the T$_{\text{R}}$ENTo model which is used to imitate the initial state of heavy-ion collisions [29]. In this study, we choose the geometric thickness function with $p = 0$. The nucleus thickness function is a superposition of the nucleon thickness function whose Gaussian width is chosen as $w = 0.5$ fm. In addition, the fluctuation of nucleon thickness function is considered by a gamma distribution with variance $1/k$ where we have chosen $k = 1$. Also, we use the same T$_{\text{R}}$ENTO parametrization for these simulations at different centrality classes to have the same situation for both deformed and spherical nuclei. To shed light on the effect of nuclear deformity on the properties of system formed after their collision, we consider three sets of deformation parameters for UU collisions as follows:

(1) $\beta_2 = 0$ and $\beta_3 = 0$: spherical U;

(2) $\beta_2 = 0.265$ and $\beta_3 = 0$: effect of β_2;

(3) $\beta_2 = 0.265$ and $\beta_3 = 0.1$: effect of β_2 and β_3.

In the previous section, it was shown that one way to study a random variable is to scrutinize its moments, cumulants, and probability distribution. We propose that, in order to obtain more insight into the impact of deformation, we need to study flow harmonics. Thus, we will compare the observables related to the collision of spherical and deformed nuclei. To show how this method works in the flow studies, we plug $t = \frac{1}{2}(t_x - it_y)$ and $Z = v_{x,n} + iv_{y,n}$ into Eq. (2) for any harmonics

[2]Since this linear response works for $n = 2, 3$ and not higher harmonics and gives us a simple picture of the relationship between initial and final states, we do not discuss higher harmonics here. The method employed here, however, works to study higher flow harmonic as well while that would be complicated.

[3]We performed the same analysis for UU collisions at 5.02 TeV center-of-mass energies and the results are exactly the same.

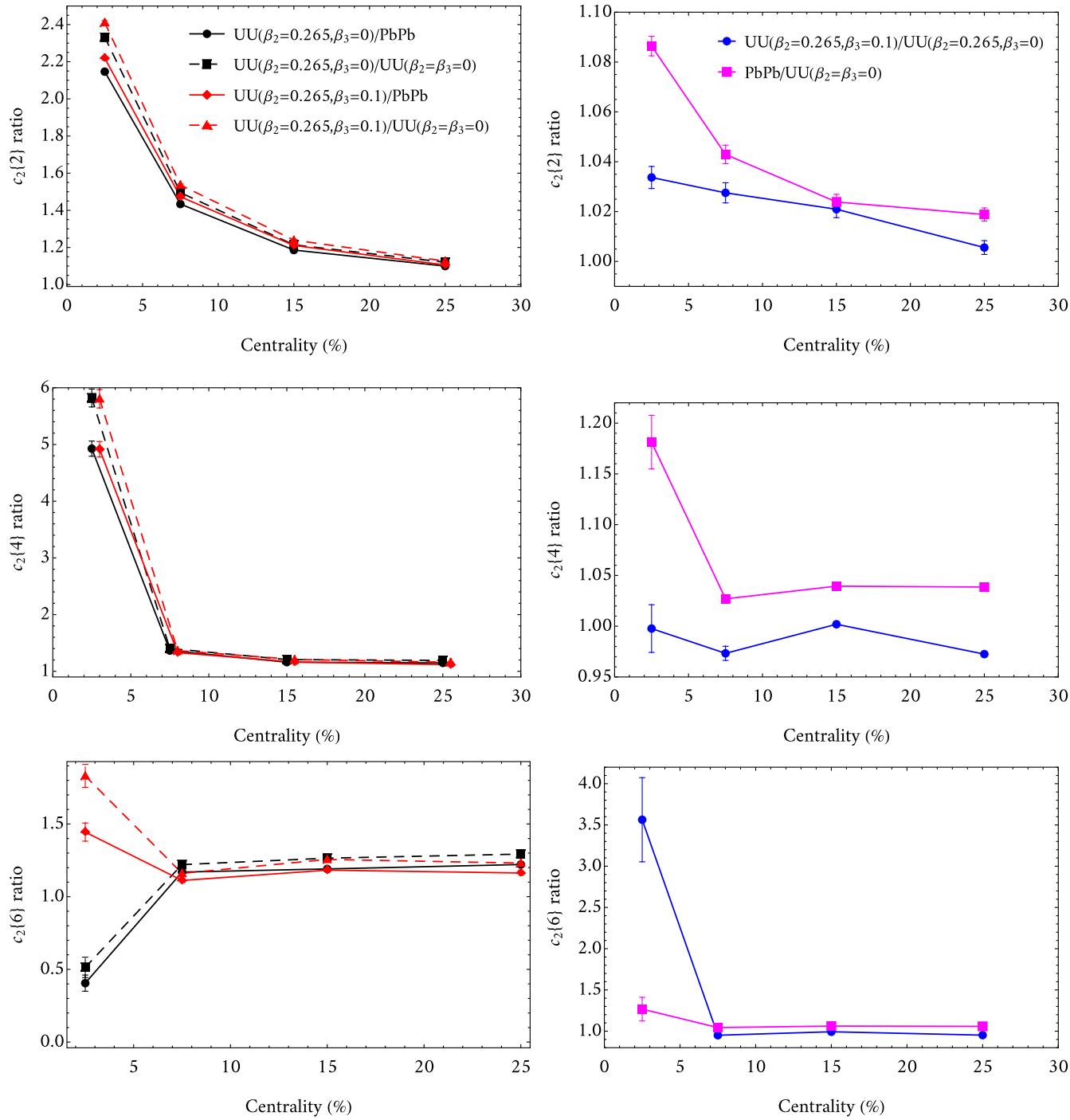

FIG. 1. In the left panels, the centrality dependence of the ratios of $2k$-particle correlation functions $c_2\{2k\}$ in the collision of deformed UU (for vanishing and nonvanishing values of β_3) to the $c_2\{2k\}$ in the collision of spherical nuclei, e.g., PbPb and UU ($\beta_2 = \beta_3 = 0$) demonstrated. In the right panels, we compare the centrality dependence of the ratio of correlation functions in collisions of UU ($\beta_2 = 0.265$, $\beta_3 = 0$) to the UU ($\beta_2 = 0.265$, $\beta_3 = 0.1$) and PbPb to the UU ($\beta_2 = \beta_3 = 0$). Data have been generated at the center-of-mass energy $\sqrt{s_{NN}} = 5.02$ TeV.

(see more details in Ref. [24]). Following these considerations, we arrive at the $2k$-particle correlation functions [15]:

$$c_n\{2\} = \langle v_n^2 \rangle, \quad c_n\{4\} = \langle v_n^4 \rangle - 2\langle v_n^2 \rangle^2, \ldots. \tag{4}$$

To examine the effect of nuclear deformity on the observables we compare the centrality dependence of the ratio of $2k$-particle correlation function $c_2\{2k\}$ (with $k = 1, 2, 3$) of the system after collision of deformed nuclei to those obtained after the collision of spherical nuclei in the left panel of Fig. 1. The maximum variation from 1 is observed at 0%–5% centrality. Furthermore, the corresponding ratios decrease with increasing impact parameter. In the right panel of this figure, we present the ratios of $c_2\{2k\}$ for UU collisions with an

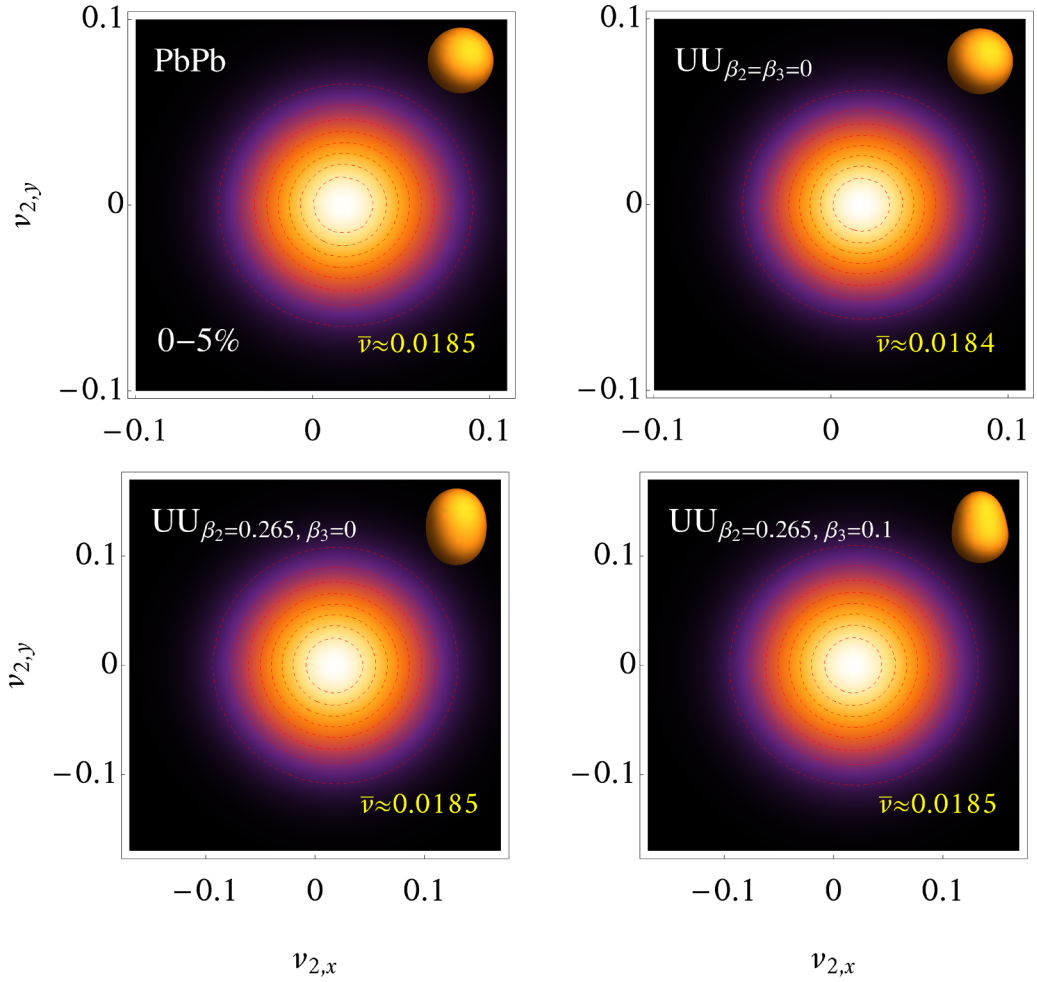

FIG. 2. The two-dimensional distribution $P(v_{2,x}, v_{2,y})$ with $v_{2,x} = \alpha_2\varepsilon_{2,x}$ and $v_{2,y} = \alpha_2\varepsilon_{2,y}$ with $\alpha_2 = 0.339$, obtained from $\mathrm{T_R ENTO}$ using the same parametrization for PbPb (top-left panel), UU($\beta_2 = 0.265$, $\beta_3 = 0$) (top-right panel), UU($\beta_2 = 0.265$, $\beta_3 = 0$) (bottom-left panel), and UU($\beta_2 = \beta_3 = 0$) (bottom-right panel). Also, the central mean values (the values of average ellipticity) $\bar{v}_2$ given for each plot. We observe that $\bar{v}_2$ is the same for all systems.

octupole and quadrupole deformation to the corresponding quantity for collision of uranium with only quadrupole deformation. We observe a deviation from 1 in the most central collisions for this ratio. This is related to the nonvanishing β_3. The maximum deviation is observed in the plot of $c_2\{6\}$ at 0%–5% centrality. Moreover, in this panel, we compare the $c_2\{2k\}$ ratios of PbPb to spherical UU collisions. There is a 8.5% deviation in the ratio $c_2\{2\}$. Note that correlation function $c_2\{2\}$ serves as the variance of elliptic flow distribution. In addition, we have approximately 18.5% and 25% deviations in the ratios of $c_2\{4\}$ and $c_2\{6\}$, respectively. Generally, although we observe the same mean value, $\bar{v} \equiv \langle v_x\rangle$ ($\langle v_y\rangle = 0$), the different structure leads to a change in the variances, and the deformation enhances this change, as can be deduced from the top panels of Fig. 1.

In Fig. 2 the two-dimensional distributions of elliptic flow $P(v_{2,x}, v_{2,y})$ for different spherical- and deformed-nucleus collisions at 0%–5% centrality is demonstrated. The values of average ellipticity $\bar{v}_2$, which measures the average value of the x component of elliptic flow, e.g., $\bar{v}_2 \equiv \bar{v} = \langle v_x\rangle$, are shown in each panel as well. As it turns out the flow distributions of flow harmonic obtained from the collision of deformed and the spherical nuclei have a different behavior due to deviation of correlation $c_2\{2\}$ ratios from 1 (see Fig. 1), while they have the same mean value.

It is known that the experimental data [30] favor the Bessel-Gaussian (BG) distribution to explain elliptic flow distribution in spherical nuclei,

$$P(v_n) = \frac{2v_n}{c_n\{2\}} e^{-\frac{v_n^2+\bar{v}_n^2}{c_n\{2\}}} I_0\left(\frac{2v_n\bar{v}_n}{c_n\{2\}}\right).$$

At this stage let us note that the shift parameter $\bar{v}$ for $n = 2$ is generated by the reaction flow. The reaction flow happens at collisions with nonzero impact parameter. One may wonder if the BG can be a suitable choice for flow distribution in the collision of deformed ion at small centralities. The data of STAR [18] show there is a noticeable difference between the measured v_2 of deformed- and spherical-nucleus collisions. This compels us to challenge our assumptions. As mentioned in Refs. [24,31], we have to consider a shift in the x direction, $Z = (v_{n,x} - \bar{v}_n) + iv_{n,y}$, where $\bar{v}_n = \langle v_{n,x}\rangle \neq 0$ for even harmonics as depicted in Fig. 2. However, this is not the case

for odd harmonics where we have $\bar{v}_{2n+1} = 0$. Imposing this change and following the previous steps, the relation between the generating functions of moments and cumulants of a complex variable is given by

$$\ln\langle e^{t^*Z}\rangle = \sum_k \frac{(tt^*)^k}{(k!)} K_n\{2k\}. \tag{5}$$

Therefore, one finds the desired order of the real cumulants $K_n\{2k\}$ [24] as follows:[4]

$$\begin{aligned} K_n\{2\} &= \langle ZZ^*\rangle, \\ K_n\{4\} &= \langle (ZZ^*)^2\rangle - 2\langle ZZ^*\rangle^2, \\ K_n\{6\} &= \langle (ZZ^*)^3\rangle + 12\langle ZZ^*\rangle^3 - 9\langle ZZ^*\rangle\langle (ZZ^*)^2\rangle. \end{aligned} \tag{6}$$

Note that cumulants $K_n\{2k\}$ contain $c_n\{2k\}$ as well as moments such as $\bar{v}_n^i\langle v_{n,x}^j v_{n,y}^l\rangle$, where $i + j + l = 2k$. We call the above correlation functions the shifted cumulants due to nonvanishing $\bar{v}_n$. At this stage it is worth noting that, under a shift of the random variable, the cumulants remain invariant. For instance, the two-particle azimuthal correlation is given by $\langle e^{in(\phi_1-\phi_2)}\rangle - \langle e^{in\phi_1}\rangle\langle e^{-in\phi_2}\rangle$ for the case of nonperfect detector [15]. It is straightforward to verify the invariance of this correlation function under the transformation of form $\phi_i \to \phi_i - \theta$ with $i = 1, 2$. As it turns out, the cumulants $\mathcal{K}_2\{2k\}$ in Eq. (6) consist of moments $\langle v_{n,x}^j v_{n,y}^l\rangle$ which are not invariant under the shift transformation. Of course, one can find the cumulants $\mathcal{K}_n\{2k\}$ are shift invariant by removing such moments. However, they are novel theoretical tools to study the structure of nuclei. In Fig. 3, we plot Eq. (6) for $n = 2$ and for both spherical and deformed collisions. As depicted in the top plot ($K_2\{2\}$) of this figure, we observe a difference between spherical- and deformed-ion collisions. In addition, the effect of octupole deformation with nonzero β_3 in UU can be seen in this plot as well. The analysis of the eccentricity as well as cumulants in the collision of isobars of Zr and Ru indicates significant modification arising from the octupole deformation [32].

For the particular cumulant $K_2\{2\}$, the of β_3 manifests itself in mid-central collisions more noticeably. It turns out the centrality dependence of cumulants for PbPb and spherical UU collisions are very similar. Concerning the next order cumulants, i.e., $K_2\{4\}$, there is a considerable difference between the magnitude of the aforementioned quantity for deformed and spherical ion collisions. We have $K_2\{4\} \approx 0$ for spherical-nucleus collisions as expected. The difference between deformed uranium collisions with and without β_3 manifests itself in $K_2\{4\}$ and $K_2\{6\}$. It can be seen the effect of β_3 is decreasing in $K_2\{6\}$, whereas increasing in $K_2\{4\}$ and $K_2\{2\}$. This difference appears more clearly in $K_2\{6\}$ compared with the $K_2\{4\}$. As demonstrated in Figs. 1 and 3, the splitting between different values of quadrupole β_2 and octupole β_3 can be obtained from the shifted cumulants $K_n\{2k\}$ in contrast with $2k$-particle correlations $c_n\{2k\}$. This

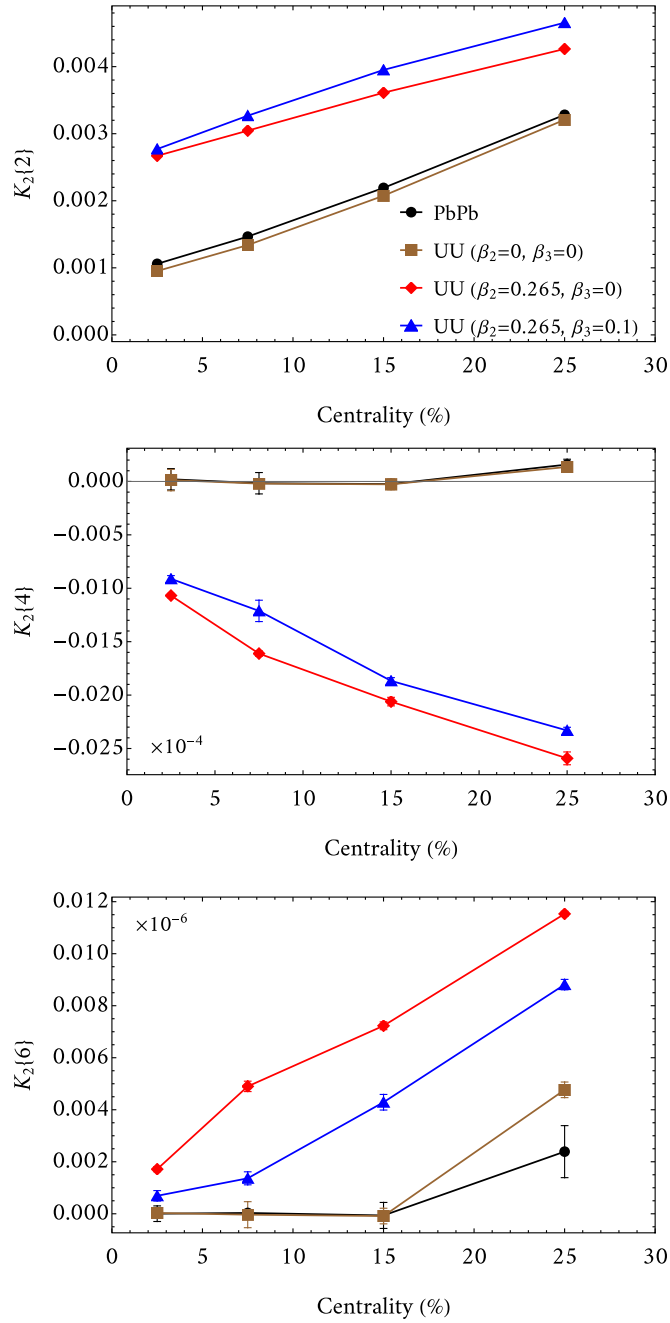

FIG. 3. The centrality dependence of the shifted cumulants $K_n\{2k\}$ with $k = 1, 2, 3$. The results show the relationship between different orders of shifted cumulants is $K_2\{2\} > K_2\{4\} > K_2\{6\}$, which is the same as $2k$-particle correlation functions.

splitting appears stronger in the higher order of $K_n\{2k\}$. In other words, the results show that if we want to study the effect of deformation on flow anisotropies, it would be helpful to investigate the shifted cumulants $K_n\{2k\}$. Also, the difference between different spherical nuclei at mid-central collisions can be extracted from $K_2\{6\}$. To see this difference, one needs to include higher-order terms of cumulants in probability distributions, which we leave to future work. Moreover, as it is shown in this plot, the cumulant $K_2\{6\}$ at mid-central

[4]Let us note that they are derived by differentiating both sides of Eq. (5) at $t_x = 0$ and $t_y = 0$. Moreover, the quantity $K_n\{2k\}$ are the two-dimensional cumulants.

collisions demonstrates different behavior for the systems formed from different spherical-nucleus collisions.

As we observed the correction $\bar{v}_n$ in our assumptions led us to extract some fascinating properties. Now we study the effect of this modification on flow distributions. As discussed in Sec. II, one can study a stochastic variable using the sGC method and its characteristic function, which gives the modification to the Gaussian distribution. Thus, using Eq. (5), we investigate the shifted flow harmonics with $Z = v_{n,x} - \bar{v}_n + iv_{n,y}$. To have an approach accessible in experiments, we should obtain a distribution for the magnitudes of flow harmonics. To do this, we find the radial distribution $P_r(v_n)$ by writing the distribution given in Cartesian coordinate in the polar coordinate and then integrating the two-dimensional distribution $P(v_{n,x}, v_{n,y})$ over the Ψ_n (see Ref. [24]) as follows:

$$\begin{aligned} P_r(v_n) &= \frac{d}{dv_n}\int P(v_x, v_y)dv_x dv_y \\ &= \frac{d}{dv_n}\int v_n P(v_n, \Psi_n)dv_n d\Psi_n, \end{aligned} \tag{7}$$

where

$$P(v_n, \Psi_n) \approx \left[1 + \sum_{k=2} \frac{R_n\{2k\}\mathcal{D}^k_{v_n,\Psi_n}}{4^k(k!)^2}\right]\mathcal{G}(v_n, \Psi_n). \tag{8}$$

Here, $\sqrt{2\pi}\sigma\mathcal{G}(z, \phi)$ is a two-dimensional (2D) Gaussian distribution with mean $\bar{v}_n$ and standard deviation $\sqrt{R_n\{2\}/2}$. Moreover, $\mathcal{D} = \partial^2_{v_n} + (1/v_n)\partial_{v_n} + (1/v_n^2)\partial^2_{\Psi_n}$.

Bearing in mind the importance of the shift parameter introduced in Eq. (6), we have to use the radial shifted cumulants $R_n\{2k\}$. This means that the cumulants in Eq. (5) are not applicable anymore. Therefore, we employ the main definition of moments,

$$\langle v_n^{2k}\rangle = \int_0^\infty v_n^{2k} P_r(v_n)dv_n, \tag{9}$$

to obtain $R_n\{2k\}$ (see Ref. [31]). To obtain an expression for $R_n\{2k\}$, we truncate Eq. (8) at desired order of k. For example, if we keep only the first term in Eq. (8), $P_r(v_n)$ would be a BG distribution:

$$P_r(v_n) \equiv BG(v_n) = \mathcal{G}(v_n; \bar{v}_n)I_0\left(\frac{2v_n\bar{v}_n}{R_n\{2\}}\right), \tag{10}$$

where

$$\mathcal{G}(v_n; \bar{v}_n) = (2v_n/R_n\{2\})\exp\left[-\frac{v_n^2 + \bar{v}_n^2}{R_n\{2\}}\right]$$

is one-dimensional (1D) Gaussian distribution with nonzero central moment, and $I_j(z)$ is the modified Bessel function of the first kind. In this case, we just have $R_n\{2\}$:

$$\langle v_n^2\rangle = \int v_n^2 P_r(v_n)dv_n = \int v_n^2 BG(v_n)dz = R_n\{2\} + \bar{v}_n^2.$$

At this stage, we obtain the form of the first shifted cumulants using the equality above as $R_n\{2\} = \langle v_n^2\rangle - \bar{v}_n^2 = c_n\{2\} - \bar{v}_n^2$. However, we can keep higher-order terms in this expansion as well to arrive at a distribution which includes corrections to Bessel-Gaussianity in Eq. (10) as $P_r(v_n) = BG(v_n) + P_k(v_n)$. Here, $P_k(v_n)$ includes corrections from higher cumulants. It is known from experiments [8] that the BG distribution presents a suitable description for the distribution of flow harmonics in collisions of spherical nuclei from most- to mid-central collisions. Now, one may wonder if we can use this expression for deformed nuclei in the same centrality classes. To answer this, we consider the correction to BG distribution which just includes the second and third radial shifted cumulants, $R_n\{4\}$ and $R_n\{6\}$, as follows:

$$\begin{aligned} P_r(v_n) &= BG(v_n) + P_2(v_n) + P_3(v_n) \\ &= \mathcal{G}(v_n; \bar{v}_n)I_0\left(\frac{2v_n\bar{v}_n}{R_n\{2\}}\right) \\ &\quad + \frac{1}{2}\gamma_4\mathcal{G}(v_n; \bar{v}_n)\sum_{j=0}^{2}\alpha_{2,j}I_j(2v_n\bar{v}_n/R_n\{2\}) \\ &\quad + \frac{1}{6}\gamma_6\mathcal{G}(v_n; \bar{v}_n)\sum_{j=0}^{3}\alpha_{3,j}I_j(2v_n\bar{v}_n/R_n\{2\}). \end{aligned} \tag{11}$$

The coefficients γ_{2k} and α_j in the correction terms of Eq. (11) are

$$\begin{aligned} \gamma_4 &= R_n\{4\}/R_n\{2\}^2, \quad \gamma_6 = R_n\{6\}/R_n\{2\}^3, \\ \alpha_{2,0} &= L_2\left(\frac{v_n^2 + \bar{v}_n^2}{R_n\{2\}}\right) + \frac{v_n^2\bar{v}_n^2}{R_n\{2\}^2}, \\ \alpha_{3,0} &= L_3\left(\frac{v_n^2 + \bar{v}_n^2}{R_n\{2\}}\right) + \frac{3v_n^2\bar{v}_n^2}{R_n\{2\}^2}L_1\left(\frac{v_n^2 + \bar{v}_n^2}{3R_n\{2\}}\right), \\ \alpha_{2,1} &= \frac{4v_n\bar{v}_n}{R_n\{2\}}L_1\left(\frac{v_n^2 + \bar{v}_n^2}{2R_n\{2\}}\right), \\ \alpha_{3,1} &= \frac{6v_n\bar{v}_n}{R_n\{2\}}L_2\left(\frac{v_n^2 + \bar{v}_n^2}{2R_n\{2\}}\right) + \frac{v_n^4 + 6v_n^2\bar{v}_n^2 + \bar{v}_n^4}{8R_n\{2\}^2}, \\ \alpha_{2,2} &= \frac{v_n^2\bar{v}_n^2}{R_n\{2\}^2}, \quad \alpha_{3,2} = \frac{3v_n^2\bar{v}_n^2}{R_n\{2\}^2}L_1\left(\frac{v_n^2 + \bar{v}_n^2}{3R_n\{2\}}\right), \\ \alpha_{3,3} &= \frac{v_n^3\bar{v}_n^3}{3R_n\{2\}^3}, \end{aligned}$$

where $L_i(z)$ are the Laguerre polynomials. Let us emphasize that we kept up to the third orders $k = 3$ since higher-order cumulants are small.[5] Moreover, as it turns out, γ_4 is the standardized kurtosis for the radial flow distribution. Note that since $\bar{v}_{2n+1} = 0$ we find odd flow kurtosis introduced in Ref. [19]. Note that, if we set $\gamma_4 = \gamma_6 = 0$, we arrive to the Bessel-Gaussian distribution. Plugging Eq. (11) into Eq. (9), the cumulants $R_n\{2k\}$ with $k = 1, 2, 3$ are given by

$$\begin{aligned} R_n\{2\} &= \langle v_n^2\rangle - \bar{v}_n^2 = c_n\{2\} - \bar{v}_n^2, \\ R_n\{4\} &= \langle v_n^4\rangle - 2\langle v_n^2\rangle^2 + \bar{v}_n^4 = c_n\{4\} + \bar{v}_n^4. \\ R_n\{6\} &= \langle v_n^6\rangle - 9\langle v_n^4\rangle\langle v_n^2\rangle + 12\langle v_n^2\rangle^3 - 4\bar{v}_n^6 = c_n\{6\} - 4\bar{v}_n^6. \end{aligned} \tag{12}$$

[5]To examine this claim, we included them and confirmed they are small and negligible.

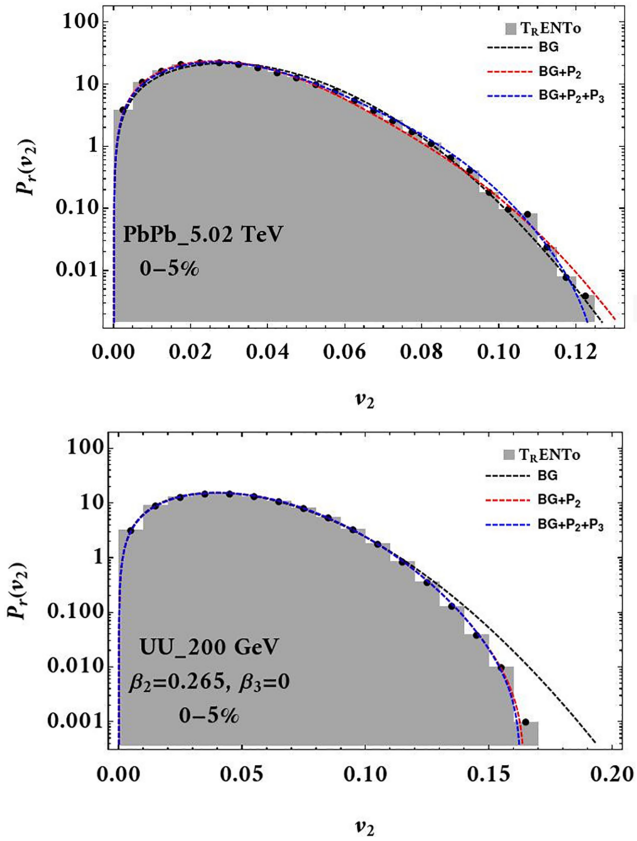

FIG. 4. A comparison of the obtained elliptic distribution with $BG(v_2)$ and different corrections P_2 and P_3 is presented by dashed black, red, and blue lines, respectively. The top panel displays the data of PbPb at 0%–5%, while the bottom panel shows the results of UU collisions in the same centrality class.

We see that $R_n\{2\} = K_n\{2\}$ as expected. So, if one obtains $R_n\{2\}$ for different collisions, the results in the top panel of Fig. 3 are reproduced. To investigate $P_r(v_n)$ for both spherical- and deformed-nucleus collisions, we focus on 0%–5% centrality where the initial geometry of produced system after the collision is inherited solely from nucleus deformity [18]. Figure 4 shows a comparison of the distribution of obtained elliptic flow from PbPb with UU collisions. As depicted in this figure, the leading-order truncation of Eq. (10) is a reliable estimation for PbPb data in most central collisions. In contrast to PbPb, the distribution of UU indicates a trace of non-Bessel-Gaussianity. This comes from the term involving $R_2\{4\}$, which is the kurtosis correction, and are comparable to the leading term in deformed UU collisions. In this context, Fig. 5 shows a noticeable difference between the values of $R_2\{4\}$ and subsequently the values of standardized kurtosis for the collisions of spherical and deformed nuclei. Furthermore, once β_3 is turned on, we observe an enhancement in the magnitude of $R_2\{4\}$ opposite to $c_2\{4\}$ and $K_2\{4\}$. If we want to investigate the deformation effect, in particular the octupole structure of nuclei, on v_3, it seems that increasing β_3 would lead to a correction to Bessel-Gaussianity as well. In Fig. 6, we show the distribution of v_3 both for PbPb and ZrZr collisions in 0%–5% centrality. The results imply that large values of β_3 play a

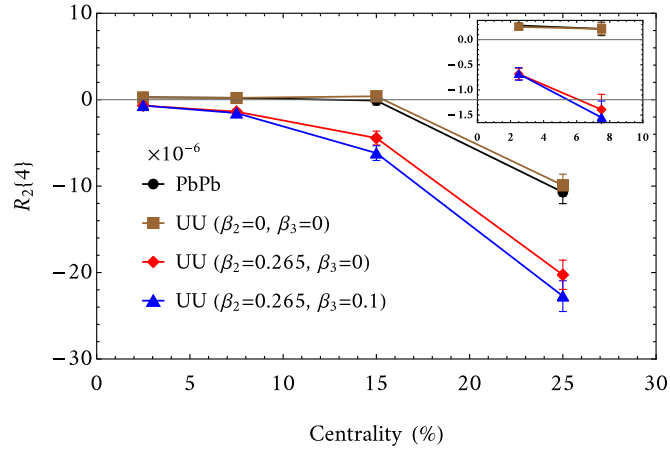

FIG. 5. Comparing the cumulants $R_2\{4\}$ as a function of centrality for different spherical- and deformed-nucleus collisions. The mini panel presents the values $R_2\{4\}$ where we expect maximum deformity.

significant role in v_3 distribution. This effect appears as a non-Bessel-Gaussian distribution, while the Bessel-Gaussian approximation works well for spherical nuclei. To study the correction part of v_3 distribution, we should investigate the coefficient $\gamma_4 = R_3\{4\}/R_3\{2\}^2$. Figure 7 shows a comparison

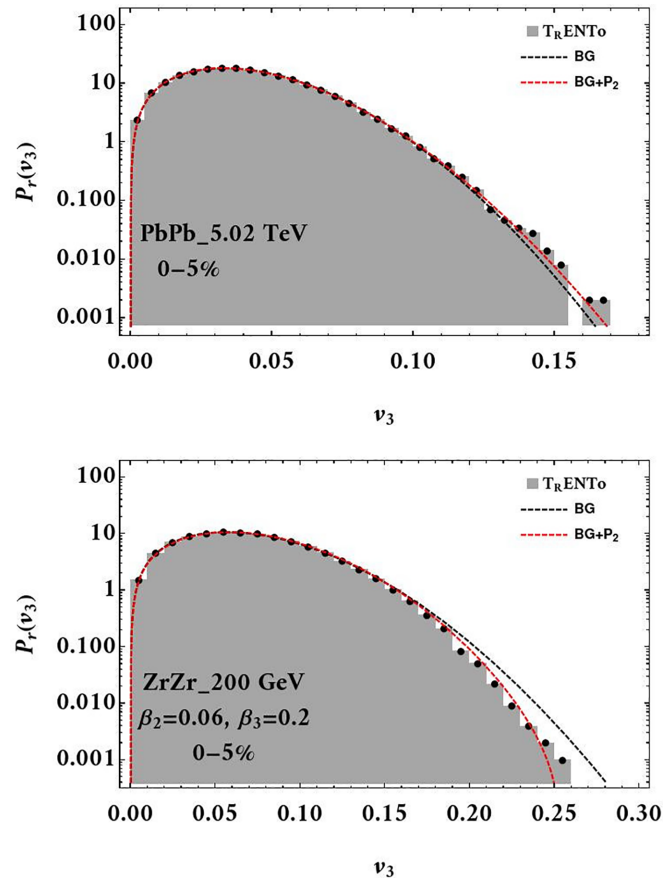

FIG. 6. Similar to Fig. 4 but for the third harmonic v_3 distribution of PbPb (top) and ZrZr (bottom) collisions.

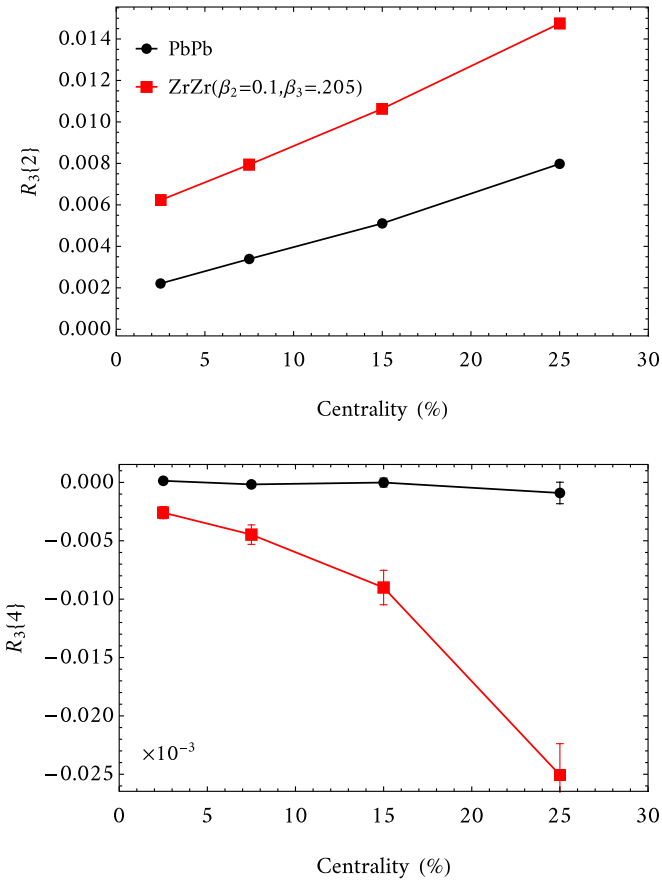

FIG. 7. The results show the values of $R_3\{2\}$ and $R_3\{4\}$, which are obtained from PbPb data and ZrZr data.

of $R_3\{2\}$ and $R_3\{4\}$ for PbPb and ZrZr collisions. Note that due to $\bar{v}_3 = 0$, one can find $R_3\{2k\} = c_3\{2k\}$, and then we reproduced kurtosis introduced in Ref. [19]. As illustrated in Fig. 7, we find that the cumulants in collisions of ZrZr have a larger magnitude than spherical ones. This leads to a non-negligible difference in the coefficient γ_4, and thus, the correction terms are crucial in ZrZr as shown in Fig. 6.

To conclude this section, let us note that, as two deformed nuclei approach and collide, the initial geometry of plasma produced after collision affected by two factor of impact parameter and the shape of nuclei. Hence, the interaction zone which forms after the collision of deformed nuclei is sensitive to nucleus shape. On the other hand, the change in the overlapping area, due to the deformation of nuclei and finite impact parameter, can have effects on the cumulants (subsequently on the kurtosis) and distributions of flow harmonics. In this regard, we believe that the standard Gram-Charlier series would be ideal tool as a probe of nuclear structure in distribution analysis.

IV. ELLIPTICITY

One of the main results from studying flow harmonics is that the averaged ellipticity $\bar{v}_{2n}$ is nonzero. This leads us to look for an accessible estimation of $\bar{v}_{2n}$ experimentally. Since we are interested in v_2 for SS and DD collisions, we present a possible approach to observe this quantity. Let us start with a 2D distribution of $(v_{2,x}, v_{2,y})$ in Fig. 2. As it turns out, there is a nonvanishing $\bar{v}_2$ for collisions of deformed as well as spherical nuclei. Despite the large size of $(v_{2,x}, v_{2,y})$ distributions for DD collisions, the values of averaged ellipticity are the same. However, the path to find the estimations of $\bar{v}_2$ for spherical- and deformed-ion collisions is different. At first, we prefer to present this estimation for deformed-nucleus collisions. To do this, we start with the closest estimate of distribution $P_r(v_2)$ for the data of deformed-deformed collisions which is given by $BG + P_2(v_2)$. This means that the higher-order correction terms, i.e., $R_2\{6\}$, are very small such that $R_2\{6\} \approx 0$. To verify this, we plotted this cumulant in Fig. 8. As demonstrated, the magnitude of $R_2\{4\}$ for various centralities is larger than $R_2\{6\}$. Moreover, at 0%–5% and 5%–10% centralities $R_2\{6\}$ is closer to zero. Therefore, we estimate the value of $R_2\{2k\}$ for $k = 1, 2, 3$ by considering

$$R_2\{2\} = c_2\{2\} - \bar{v}_2^2 \approx 0 \Rightarrow \bar{v}_2\{2\} \approx (c_2\{2\})^{1/2},$$

or

$$R_2\{4\} = c_2\{4\} + \bar{v}_2^4 \approx 0 \Rightarrow \bar{v}_2\{4\} \approx (-c_2\{4\})^{1/4},$$

or

$$R_2\{6\} = c_2\{6\} - 4\bar{v}_2^6 \approx 0 \Rightarrow \bar{v}_2\{6\} \approx (c_2\{6\}/4)^{1/6}. \quad (13)$$

Note that $c_2\{2k\}$ in the right-hand side of Eq. (13) are the $2k$-particle correlation functions which can be measured experimentally. This means that the ellipticity $\bar{v}_2$ could be obtained experimentally as well. Focusing on the first condition, we find that in this case all the γ_{2k} in Eq. (11) diverge unless $R_2\{2k\} = 0$. This leads to finding a δ function for $P(v_{2,x}, v_{2,y})$, thus it is not compatible with the experimental observation. As the middle panel in Fig. 8 depicts, $\bar{v}_2\{2\}$ is not a suitable candidate of $\bar{v}_2$. Having a Bessel-Gaussian distribution is the result of choosing the second line [33]. This implies a zero kurtosis, $\gamma_4 = 0$, and then the behavior of distributions obtained from spherical- and deformed-nucleus collisions is similar and we see no effect of nucleus deformity using distribution analysis. This is in contrast with our conclusion so far. The mini panel in the middle plot of Fig. 8 indicates this estimation is not accurate at most central collisions. Of course, $\bar{v}_2\{4\}$ is a suitable choice to estimate averaged ellipticity at large centralities. Finally, we arrive at the last line of Eq. (13). This implies a truncation at $k = 2$. This is in agreement with our results in Sec. III. Moreover, we find $\gamma_6 \approx 0$. As it turns out, after some straightforward manipulation in the last line of Eq. (13), the standardized kurtosis γ_4 is given by

$$\gamma_4 \approx -(v_2\{4\}^4 - v_2\{6\}^4)/(v_2\{2\}^2 - v_2\{6\}^2)^2. \quad (14)$$

This implies a fine splitting between $v_2\{4\}$ and $v_2\{6\}$ due to nonzero value of γ_4 in deformed-nucleus collisions [26]. The bottom panel in Fig. 8 implies a difference on the γ_4 for systems with and without nonzero triangular deformation β_3.

To conclude this section, the closest estimate of $\bar{v}_2$ is given by $\bar{v}_2\{6\}$. In contrast with $\bar{v}_2\{4\}$, only $\bar{v}_2\{6\}$ explains $\bar{v}_2$ at most central collisions where the maximum deformity is expected to be observed. Since PbPb data can be explained by the BG distribution, we find that $\bar{v}_{2,S} = \bar{v}_{2,S}\{4\}$. Concerning

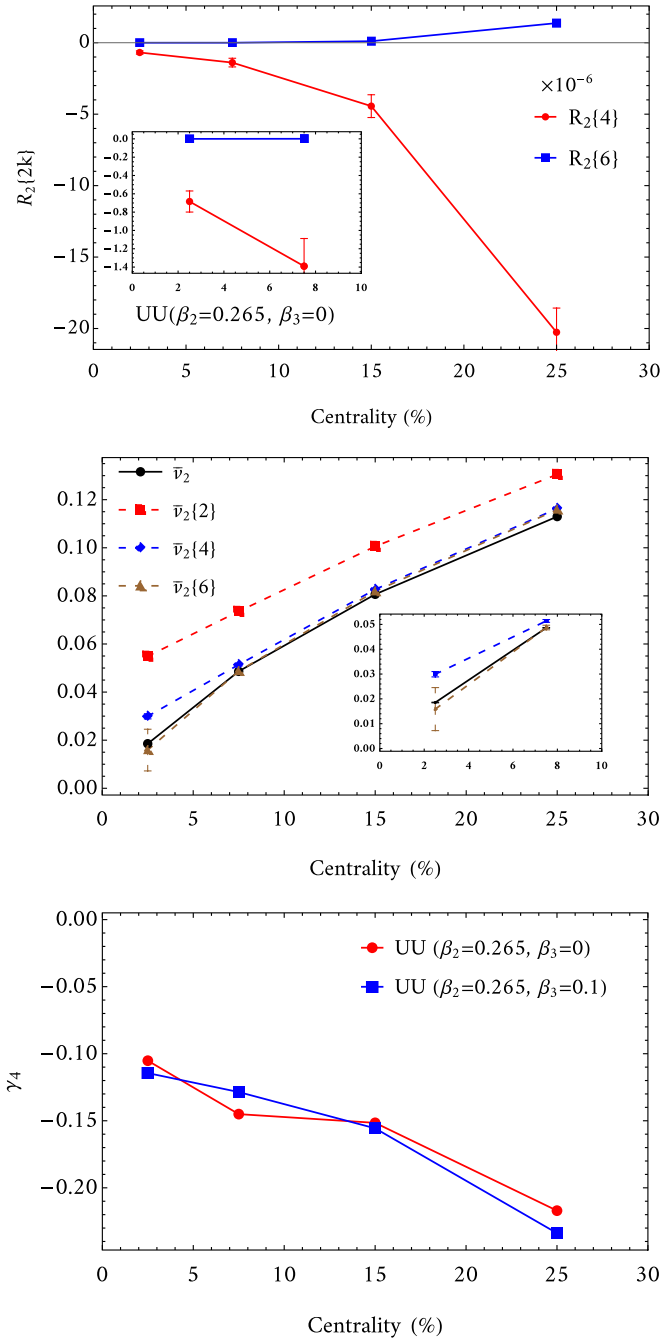

FIG. 8. Here we show a comparison of $R_2\{4\}$ with $R_2\{6\}$ (in the top panel), the estimated values of $\bar{v}_2$ for different collisions (in the middle panel), and the standardized kurtosis γ_4 obtained in Eq. (14) (in the bottom panel) as a function of centrality.

this argument and derived relation $\bar{v}_D \approx \bar{v}_S$ in the Appendix, one arrives at $\bar{v}_{2,D} = \bar{v}_{2,D}\{6\} = \bar{v}_{2,S}\{4\}$ as well. This enables us to determine the averaged ellipticity of deformed-nucleus collisions with the observables of spherical-ion collisions.

V. CONCLUSIONS

Motivated by the collisions of deformed nuclei, in this paper, we studied the flow distribution in the collisions of the spherical and deformed nuclei. In the first part of this paper, we presented a systematic approach to calculate the corresponding cumulants for spherical- and deformed-ion collisions. It was shown that, in the most central collisions, the ratios of the $2k$-particle correlation function $c_2\{2k\}$ in the collision of deformed nuclei to the corresponding quantity in the collision of spherical nuclei manifest the effect of nuclear deformity more clearly. To be able to distinguish between the cumulants of different collisional systems, we considered the effect of the shift parameter $\bar{v}_n$. Then, we scrutinized the effect of different forms of deformation, including quadrupole β_2 as well as octupole β_3, through the shifted cumulants. We observed that the shift parameter manifests clearly the differences between the cumulants in the collisions of deformed and spherical nuclei.

Concerning the effect of nuclear deformity on the distribution of flow harmonics in the HIC, we then calculated the desired quantity. It was shown, after keeping an appropriate number of terms, that the resulting distribution described the data very well. Comparing the flow distribution in the collision of deformed and spherical nuclei reveals the effect of various kinds of deformation on flow harmonics.

Finally, we discussed a possible way to measure the shift parameter through the analysis of different radial cumulants for deformed nuclei in central collisions. We observed for deformed nuclei the most appropriate choice is the measurement of $\bar{v}_2\{6\}$ whereas for the collisions of spherical nuclei $\bar{v}_2\{4\}$ is an appropriate choice. It would be interesting to extend this work to the collision of Ru-Ru and Zr-Zr using full hydrodynamic simulations which are more relevant for the isobar program. The aim of such studies is to extract the effect related to CME from the background. We postpone these subjects to future studies.

ACKNOWLEDGMENTS

We thank Jiangyong Jia and Giuliano Giacalone for their useful comments. We are thankful to Wilke van der Schee for helpful discussions and invaluable feedback. H.M. thanks CERN-TH group for the support. H.M. is funded by the Cluster of Excellence *Precision Physics, Fundamental Interactions, and Structure of Matter* (PRISMA$^+$ EXC 2118/1) funded by the German Research Foundation (DFG) within the German Excellence Strategy (Project ID 39083149).

APPENDIX: RELATION BETWEEN OBSERVABLES

In Sec. III, we presented the comparison in the flow distribution of spherical- and deformed-nucleus collisions as a probe of nuclear structure. We showed that the effect of deformation appears for the second and third harmonics. It is useful to have an estimate of the observables in the collision of deformed nuclei. Thus, we want to estimate the observables by fitting a known spherical-spherical distribution, e.g., PbPb, to the deformed-nucleus data like UU. To do that, we need to modify the flow distribution obtained in the collision of spherical nuclei. Since the correction included at $k = 3$ is negligible, we keep the modification of $P_r(v_n)$ in Eq. (11) at

$k = 2$:

$$P_r^M(v_n) = \mathcal{G}(v_n'; \bar{v}_{\rm est}) I_0(2v_n'\bar{v}_{\rm est}/R_n\{2\}_{\rm est}) + \frac{1}{2}\gamma_4^{\rm est}\mathcal{G}(v_n'; \bar{v}_{\rm est}) \sum_{j=0}^{2} \alpha_{2,j}^{\rm est}(v_n') I_j(2v_n'\bar{v}_{\rm est}/R_n\{2\}_{\rm est}). \tag{A1}$$

Inspired by Refs. [34,35], the estimated parameters in the above are defined by

$$v_n' = v_{n,0} + \sum_{m=2} p_m\beta_m, \quad \bar{v}_{\rm est} = \bar{v}_0 + \sum_{m=2}\delta_{1,m}\beta_m,$$
$$R_n\{2\}_{\rm est} = R_n\{2\}_0 + \left(\sum_{m=2}\delta_{2,m}\beta_m\right)^2,$$
$$R_n\{4\}_{\rm est} = R_n\{4\}_0 + \left(\sum_{m=2}\delta_{3,m}\beta_m\right)^4, \tag{A2}$$

where the index 0 in the above indicates spherical observables. In fact, Eq. (A2) is the simplest case to study the impact of deformation directly in terms of observables. However, this modification allows us to study the effect of deformation directly, in analogy to Ref. [34]. Here, we show that having the cumulants obtained from PbPb data, one arrives at the UU observables using Eqs. (A1) and (A2). To do this, we show that the flow distribution obtained in the collision of PbPb nuclei is same as the one seen in the spherical UU collision. In the top panel of Fig. 9, we plot the flow distribution in the collision of spherical uranium with the vanishing deformation parameter $\beta_2 = \beta_3 = 0$. It is obvious that the BG distribution can explain the data for the spherical uranium accurately. In the middle panel of this plot, the comparison in the flow distribution of PbPb and spherical uranium shows good agreement between them. This allows us to estimate the observables in collisions of deformed UU using PbPb data. Since we want to study quadrupole deformation of nuclei, as a simple case study, we generate UU collisions by setting $\beta_2 = 0.265$ and $\beta_3 = 0$. This is because of removing the β_3 effect on the cumulants $R_2\{2k\}$. As illustrated in the middle plot of Fig. 9, there is a noticeable difference between the distributions of the obtained elliptic flow form the data of spherical- and deformed-ion collisions. It should be mentioned that truncation at $k = 2$ was considered for both spherical- and deformed-ion collisions. Finding the coefficients p and δ_i leads us to the flow distribution in the collisions of deformed nuclei. Since we just considered nonzero β_2, we rename the coefficients in Eq. (A2) as $p = p_2$, $\delta_{1,\rm est} = \delta_{1,2}$, $\delta_{2,\rm est} = \delta_{2,2}^2$, and $\delta_{3,\rm est} = \delta_{3,2}^4$. As demonstrated in the bottom panel of Fig. 9, we found different estimations of UU distribution as follows:

$$P_{\rm est}^{DD} = P^M(p, \delta_{1,\rm est}, \delta_{2,\rm est}, \delta_{3,\rm est}),$$
$$P_{\rm est}^{DD} = P^M(0, \delta_{1,\rm est}, \delta_{2,\rm est}, \delta_{3,\rm est}). \tag{A3}$$

Results show that the estimated distributions are compatible with the v_2 distribution obtained from UU data qualitatively. In other words, the definitions in Eq. (A2) worked. To find their consistency, one can investigate them in other centralities. The values of coefficients $\delta_{i,\rm est}$ are presented in Table I at

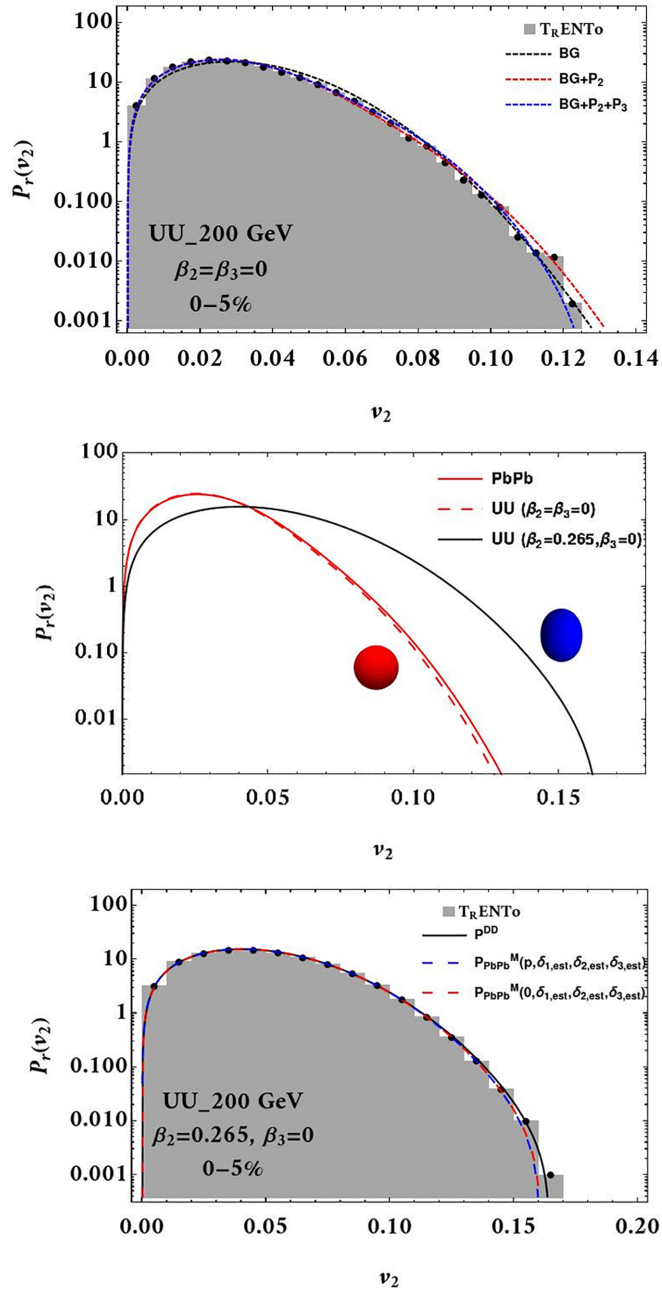

FIG. 9. In the top panel, the different corrections of spherical uranium in most-central collisions are compared. In the middle panel, the flow distribution in the collision of spherical nuclei are compared with the flow distribution in the collision of deformed uranium. The bottom panel shows different estimations of DD using the SS distribution.

TABLE I. The estimated coefficients in Eq. (A2) are shown at different centralities.

%	$\delta_{1,\rm est}$	$\delta_{2,\rm est}$	$\delta_{3,\rm est}$
0–5	0.014 ± 0.008	0.020 ± 0.001	−0.00019 ± 0.00002
5–10	0.0010 ± 0.0001	0.0224 ± 0.0004	−0.00044 ± 0.00003
10–20	0.0088 ± 0.0006	0.0167 ± 0.0003	−0.00043 ± 0.00003
20–30	0.0197 ± 0.0006	0.0039 ± 0.0002	0.00145 ± 0.00003

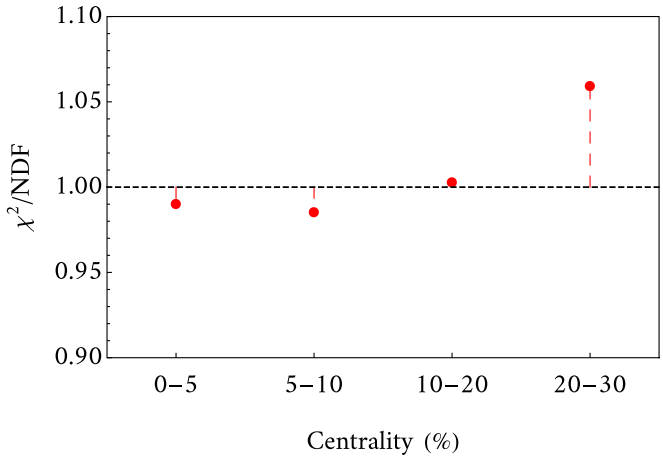

FIG. 10. χ^2/NDF values of fitting the distribution $P_r^M(v_2)$ to simulation data as function of centrality.

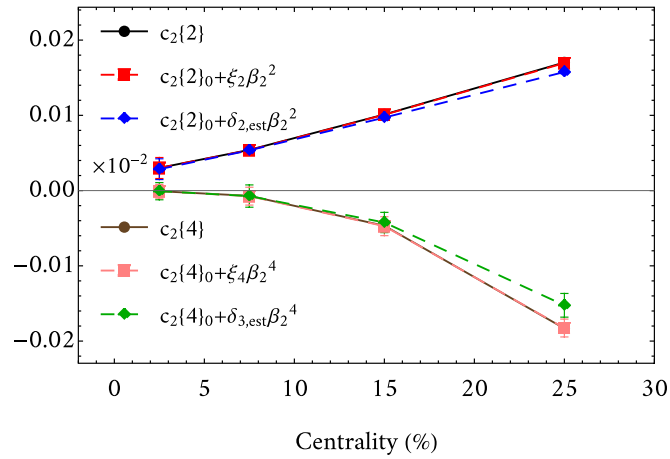

FIG. 11. Comparison of $c_2\{2\}$ and $c_2\{4\}$ obtained from DD data with their estimates using SS. The value of $c_2\{4\}$ was multiplied by 100.

different centrality classes. We see the effect of deformation would be different in each centrality due to various estimated values. Also, χ^2/NDF of fitting in each centrality are illustrated in Fig. 10. Since these values are closer to 1, one can interpret that Eqs. (A1) and (A2) present a good estimation of observables in collisions of deformed uranium. Of course, the value of χ^2/NDF in mid-central collisions is increasing. This means that, if we go to higher centralities we need to make other truncations in Eq. (8), e.g., keep the terms included $R_n\{6\}$, $R_n\{8\}$ and so on to explain the data without any fitting. Moreover, in order to study the $2k$-particle correlation functions $c_n\{2k\}$ in the collision of deformed nuclei, we have to consider an expansion of the form

$$c_n\{2k\}_{\mathrm{est}} = c_n\{2k\}_0 + \left(\sum_{m=2}\xi_{2k,m}\beta_m\right)^{2k}. \tag{A4}$$

As mentioned in Eq. (12), $R_n\{2k\}_{\mathrm{est}}$ is a function of $c_n\{2k\}_{\mathrm{est}}$ and $\bar{v}_{n,\mathrm{est}}$. Plugging Eq. (A4) in Eq. (12) and separating the terms with β_n from spherical terms, one can find the following relations:

$$\begin{aligned}
R_n\{2\}_{\mathrm{est}} &= R_n\{2\}_0 - \left(\sum_{m=2}\delta_{1,m}\beta_m\right)^2 \\
&\quad - 2\left(\sum_{m=2}\delta_{2,m}\beta_m\right)\bar{v}_0 + \left(\sum_{m=2}\xi_{2,m}\beta_m\right)^2, \\
R_n\{4\}_{\mathrm{est}} &= R_n\{4\}_0 + \left(\sum_{m=2}\delta_{1,m}\beta_m\right)^4 \\
&\quad + 4\left(\sum_{m=2}\delta_{1,m}\beta_m\right)^3\bar{v}_0 + 6\left(\sum_{m=2}\delta_{1,m}\beta_m\right)^2\bar{v}_0^2 \\
&\quad + 4\left(\sum_{m=2}\delta_{1,m}\beta_m\right)\bar{v}_0^3 + \left(\sum_{m=2}\xi_{4,m}\beta_m\right)^4,
\end{aligned} \tag{A5}$$

keeping in mind that $R_n\{2\}_0 = c_n\{2\}_0 - \bar{v}_{n,0}^2$ and $R_n\{4\}_0 = c_n\{4\}_0 + \bar{v}_{n,0}^4$. Now, we obtain $\xi_{2k,m}$ by equating Eqs. (A2) and (A5). Since we are interested in β_2 terms, we seek an expression for $\xi_{2k,2}$ as a function of δ and β_2. This is given by

$$\begin{aligned}
\xi_2 \equiv \xi_{2,2}^2 &= \delta_{1,2}^2 + \delta_{2,2}^2 + 2\frac{\delta_{1,2}\bar{v}_{2,0}}{\beta_2}, \\
\xi_4 \equiv \xi_{4,2}^4 &= -\delta_{1,2}^4 + \delta_{3,2}^4 - 4\frac{\delta_{1,2}^3\bar{v}_{2,0}}{\beta_2} \\
&\quad - 6\frac{\delta_{1,2}^2\bar{v}_{2,0}^2}{\beta_2^2} - 4\frac{\delta_{1,2}\bar{v}_{2,0}^3}{\beta_2^3}.
\end{aligned} \tag{A6}$$

Plugging $\delta_{1,\mathrm{est}} = \delta_{1,2}$, $\delta_{2,\mathrm{est}} = \delta_{2,2}^2$, and $\delta_{3,\mathrm{est}} = \delta_{3,2}^4$ in Eq. (A6) we arrive at

$$\begin{aligned}
\xi_2 \equiv \xi_{2,2}^2 &= \delta_{1,\mathrm{est}}^2 + \delta_{2,\mathrm{est}} + 2\frac{\delta_{1,\mathrm{est}}\bar{v}_{2,0}}{\beta_2}, \\
\xi_4 \equiv \xi_{4,2}^4 &= -\delta_{1,\mathrm{est}}^4 + \delta_{3,\mathrm{est}} - 4\frac{\delta_{1,\mathrm{est}}^3\bar{v}_{2,0}}{\beta_2} \\
&\quad - 6\frac{\delta_{1,\mathrm{est}}^2\bar{v}_{2,0}^2}{\beta_2^2} - 4\frac{\delta_{1,2}\bar{v}_{2,0}^3}{\beta_2^3}.
\end{aligned} \tag{A7}$$

For the particular values listed in Table I, the coefficients ξ_2 and ξ_4 are found.

We plot the $c_2\{2\}$ and $c_2\{4\}$ in Fig. 11. In this plot, the solid black and brown represent the true centrality dependence of the aforementioned quantities. Moreover, the dashed red and pink lines are derived from our estimation. There is a good agreement between the true and estimated values. Moreover, this figure shows that if we consider $\xi_2 \approx \delta_{2,\mathrm{est}}$ (blue dashed line) and $\xi_4 \approx \delta_{3,\mathrm{est}}$ (green dashed line), we can find a reasonable approximation for them from 0% to 20% centralities. Plugging Eq. (A4) into (A2) and using the approximation described, we obtain

$$R_2\{2k\}_D - R_2\{2k\}_0 = c_2\{2k\}_D - c_2\{2k\}_0. \tag{A8}$$

This leads to the same value of averaged ellipticity for both spherical- and deformed-ion collisions, i.e., $\bar{v}_D \approx \bar{v}_S$ (see Sec. IV). Let us note that the nuclei considered here have a close mass number. thus, we could perform this analysis.

To compare the observables obtained from deformed-nucleus collisions with those of spherical-spherical collisions, we study the ratio of $2k$-particle correlation functions:

$$\frac{c_2\{2\}_D}{c_2\{2\}_0} = 1 + \frac{\xi_2\beta_2^2}{c_2\{2\}_0},$$
$$\frac{c_2\{4\}_D}{c_2\{4\}_0} = 1 + \frac{\xi_4\beta_2^4}{c_2\{4\}_0}. \quad \text{(A9)}$$

Keep in mind that we have only considered the quadrupole deformation in Eq. (A4). Using the generated data for both spherical (i.e., PbPb) and deformed-nucleus (i.e., UU) collisions, we obtain $c_2\{2\}_D/c_2\{2\}_0 \approx 2$ and $c_2\{4\}_D/c_2\{4\}_0 \approx -5$ at 0%–5% centrality. The values imply that we have $c_2\{2\}_0 \approx \xi_2\beta_2^2$ and $c_2\{4\}_0 \approx (-1/6)\xi_4\beta_2^4$. The effect of deformation on two- and four-particle correlation functions is significant and cannot be ignored.

[1] K. H. Ackermann *et al.* (STAR Collaboration), Phys. Rev. Lett. **86**, 402 (2001).
[2] R. A. Lacey (PHENIX Collaboration), Nucl. Phys. A **698**, 559 (2002).
[3] I. C. Park *et al.* (PHOBOS Collaboration), Nucl. Phys. A **698**, 564 (2002).
[4] K. Aamodt *et al.* (ALICE Collaboration), Phys. Rev. Lett. **105**, 252302 (2010).
[5] K. Aamodt *et al.* (ALICE Collaboration), Phys. Rev. Lett. **107**, 032301 (2011).
[6] S. Chatrchyan *et al.* (CMS Collaboration), Phys. Rev. C **87**, 014902 (2013).
[7] G. Aad *et al.* (ATLAS Collaboration), Phys. Lett. B **707**, 330 (2012).
[8] G. Aad *et al.* (ATLAS Collaboration), Eur. Phys. J. C **74**, 3157 (2014).
[9] M. Luzum and P. Romatschke, Phys. Rev. C **78**, 034915 (2008); **79**, 039903 (2009).
[10] J. Y. Ollitrault, Phys. Rev. D: Part. Fields **46**, 229 (1992).
[11] B. Schenke, P. Tribedy, and R. Venugopalan, Phys. Rev. Lett. **108**, 252301 (2012).
[12] M. Miller and R. Snellings, arXiv:nucl-ex/0312008.
[13] J. Jia and S. Mohapatra, Phys. Rev. C **88**, 014907 (2013).
[14] G. Aad *et al.* (ATLAS Collaboration), J. High Energy Phys. 11 (2013) 183.
[15] N. Borghini, P. M. Dinh, and J. Y. Ollitrault, Phys. Rev. C **64**, 054901 (2001).
[16] B. Bally, J. D. Brandenburg, G. Giacalone, U. Heinz, S. Huang, J. Jia, D. Lee, Y. J. Lee, W. Li, C. Loizides *et al.*, arXiv:2209.11042.
[17] P. Moller and A. Iwamoto, Nucl. Phys. A **575**, 381 (1994); **577**, 833 (1994).
[18] L. Adamczyk *et al.* (STAR Collaboration), Phys. Rev. Lett. **115**, 222301 (2015).
[19] N. Abbasi, D. Allahbakhshi, A. Davody, and S. F. Taghavi, Phys. Rev. C **98**, 024906 (2018).
[20] M. G. Kendall, *The Advanced Theory of Statistics* (Charles Griffinand Company, London, 1945).
[21] H. Cramer, *Mathematical Methods of Statistics*, Princeton Mathematical Series No. 9 (Princeton University Press, Princeton, 1946).
[22] W. Krzanowski, *Principles of Multivariate Analysis*, Oxford Statistical Science Series (Oxford University Press, Oxford, 2000).
[23] S. A. Voloshin, A. M. Poskanzer, A. Tang, and G. Wang, Phys. Lett. B **659**, 537 (2008).
[24] H. Mehrabpour, Phys. Rev. C **102**, 064907 (2020).
[25] G. Giacalone, J. Noronha-Hostler, M. Luzum, and J. Y. Ollitrault, Phys. Rev. C **97**, 034904 (2018).
[26] G. Giacalone, Phys. Rev. C **99**, 024910 (2019).
[27] G. Giacalone, Phys. Rev. Lett. **124**, 202301 (2020).
[28] ALICE Collaboration, arXiv:2204.10148.
[29] J. S. Moreland, J. E. Bernhard, and S. A. Bass, Phys. Rev. C **92**, 011901(R) (2015).
[30] M. Aaboud *et al.* (ATLAS Collaboration), J. High Energy Phys. 01 (2020) 051.
[31] H. Mehrabpour and S. F. Taghavi, Eur. Phys. J. C **79**, 88 (2019).
[32] C. Zhang and J. Jia, Phys. Rev. Lett. **128**, 022301 (2022).
[33] J. Jia, G. Giacalone, and C. Zhang, Phys. Rev. Lett. **131**, 022301 (2023).
[34] J. Jia, Phys. Rev. C **105**, 014905 (2022).
[35] J. Jia, Phys. Rev. C **105**, 044905 (2022).